High Frequency AC Inductor Analysis and Design for Dual Active Bridge (DAB) Converters

Zhang, Zhe; Andersen, Michael A. E.

Published in:
Proceedings of IEEE Applied Power Electronics Conference 2016

Link to article, DOI:
10.1109/APEC.2016.7468006

Publication date:
2016

Document Version
Peer reviewed version

High Frequency AC Inductor Analysis and Design for Dual Active Bridge (DAB) Converters

Zhe Zhang and Michael A. E. Andersen
Department of Electrical Engineering
Technical University of Denmark
Kgs. Lyngby, DENMARK
zz@elektro.dtu.dk and ma@elektro.dtu.dk

***Abstract*—The dual active bridge (DAB) converter is an isolated bidirectional dc-dc topology which is the most critical part for the power conversion systems such as solid-state transformers (SST). This paper focuses on analysis and design of high frequency ac inductors which are the power interfacing component in DAB converters or DAB's derivative topologies for transferring energy between the primary and secondary sides. The DAB converter's operation principles, and the corresponding voltage and current stresses over its ac inductor are analyzed. Hereby, six diverse winding arrangements are studied in order to find a design having the lowest ac resistance and core loss. Core loss is calculated by both GSE and iGSE methods, and then the results are compared under two operating conditions. Based upon the finite element method (FEM) simulation, winding losses are investigated. Finally, the case in which the core loss and the winding loss are almost equal is selected as the optimal one. The experimental results are presented to verify the validity of the analysis and design.**

Keywords—ac inductor; converter; dual active bridge; FEM; winding loss

I. INTRODUCTION

Bidirectional dc-dc converters have been attracting attention and becoming a research focus in the recent years, along with the ceaseless development and application of renewable energy systems in which a proper energy storage element and its corresponding power electronic converters are needed [1]-[6]. The dual active bridge converter (DAB), as an isolated bidirectional converter, has been proposed for over two decades. Due to its simple circuitry, symmetrical structure, low number of magnetic components and absence of bulky dc inductors, the DAB converter is considered to be a suitable candidate to carry out voltage conversion and galvanic isolation with high power density and high power efficiency, in particular, for high power applications such as solid-state transformers, electric tractions and battery interfacing circuits [7]-[9].

With regard to magnetic components of DAB converters, as a DAB topology illustrated in Fig. 1, only one high frequency transformer is adopted and its leakage inductance can be used as L_{ac} to interface the power transferring between the primary and secondary sides of the high frequency transformer. However, for many relatively low power applications in which

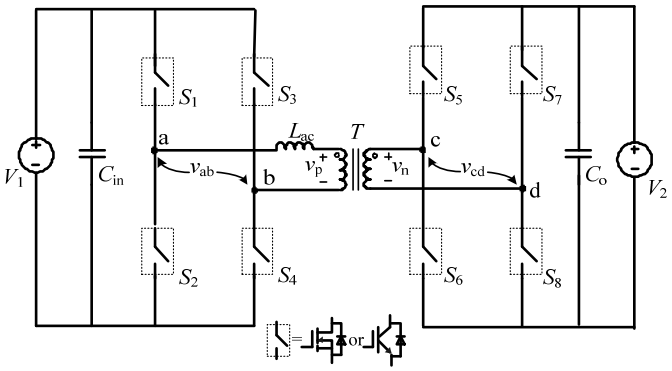

Fig. 1: Topology of the dual active bridge (DAB) converter.

if the input and output voltages are high, an external inductor to provide larger interfacing inductance is needed in order to adjust the output power as well as to extend the zero voltage switching (ZVS) operation. Of course, rather than using an extra inductive component to get larger inductance, the leakage inductance can be increased by weaken the coupling effect between the transformer windings, but the price is that the transformer winding ac resistance cannot be minimized effectively and more severe radiated EMI issues may occur. Therefore, it is more efficient to utilize external inductors instead. Diverse from filtering inductors in Buck-derived or Boost-derived dc-dc converters, here, a high frequency ac inductor which operates at the switching frequency is needed in DAB converters. For ac inductors that only carry high frequency ac current without any dc offset, the core selection and winding design have the issues very similar to that of transformer design but with one more difficulty, i.e. there are no secondary windings which can be used to reduce the proximity effect by interleaving. For the core selection, ac flux component causes core losses and potentially contributes to eddy current losses if air gaps and windings are in a close proximity. Iron powered cores cannot be used due to their relatively high core loss compared to their ferrite counterparts; on the other hand, a ferrite core with a lumped gap will have unacceptably high winding losses due to the fringing effect. These issues actually challenge designing highly efficient ac inductor, on which this paper will focus.

This paper is organized as follows. After this introduction, the special design requirements for ac inductors employed in

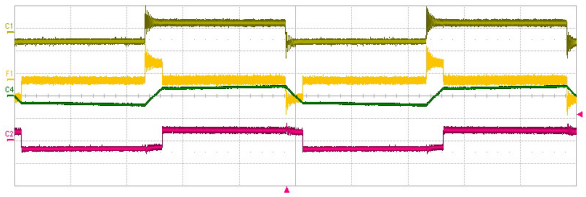

Fig. 2: Experimental waveforms of DAB converter. Ch1: v_{ab} (100V/div), Ch2: v_p (100 V/div), F1: v_L (100 V/div) and Ch4: i_L (50 A/div).

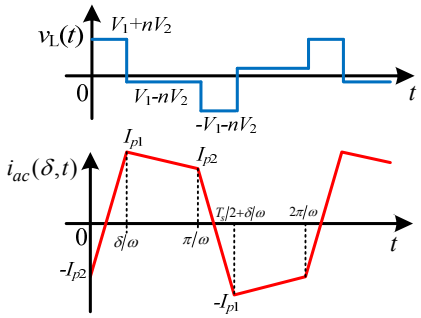

Fig. 3: Typical waveforms of ac inductor of DAB converters.

DAB converters are introduced in Section II. By using finite element method (FEM) simulation, ac inductors with six variant winding arrangements are analyzed and compared in Section III. The measurement results are presented in Section IV. Finally, the conclusion is given in Section V.

II. AC INDUCTOR IN DAB CONVERTERS

In the cases, in particular for the low power applications (below 10 kW), the leakage inductance of the high frequency transformer is not sufficient to keep DAB converters operating under ZVS conditions and the deadband effect will emerge that leads to even worse EMI noise. Therefore, an external ac inductor is needed.

A. Typical operation principle of DAB converters

As the DAB converter shown in Fig. 1, the bidirectional switch cells, i.e. S_1~S_8, are used to control reversible power between the terminals V_1 and V_2, with a phase-shift modulation. The primary and secondary full bridges with 50% duty cycle to achieve a rectangular voltage v_{ab} and v_{cd}, which have a phase-shift angle δ used as a power regulation parameter. By controlling the phase shift with a range of $-\pi\leq\delta\leq\pi$, the transferred power is then regulated as,

$$P = P_1 = P_2 = \frac{n \cdot V_1 \cdot V_2 \cdot \delta \cdot (\pi - |\delta|)}{2\pi^2 f_s L_s} \tag{1}$$

where L_s represents inductance of the ac inductor L_{ac}; f_s is the switching frequency, and n is the transformer turn ratio defined as N_p:N_s.

Therefore from the typical experimental voltage and current waveforms of the ac inductor as illustrated in Fig. 2, the more specifically theoretical waveforms, i.e. the voltage across the ac inductor and the ac inductor current, can be plotted in Fig. 3. As derived in [2], if $V_1=nV_2$, the ac inductor current i_{Lac} can be expressed by Fourier series,

$$i_{Lac} = \sum_{n=1,3,5...}^{\infty} \frac{4}{m^2 \pi \omega L_s n} \left(\sin\frac{m\delta}{2}\right) \cdot \sin\left(m\omega t - \frac{m\delta}{2}\right). \tag{2}$$

Whereas, if $V_1\neq nV_2$, a more general expression of i_{Lac} can be obtained.

$$i(\delta,t) = \sum_{m=1,3,5...}^{\infty} \frac{4}{m^2 \pi \omega L_s} \cdot [nV_2 \cdot \cos m\delta - V_1] \cdot \cos m\omega t + \sum_{m=1,3,5...}^{\infty} \frac{4}{m^2 \pi \omega L_s} \cdot nV_2 \cdot \sin m\delta \cdot \sin m\omega t. \tag{3}$$

From (3), it can be seen that there is no even-order harmonics existing in the ac current waveform and the harmonic magnitudes vary with the phase-shift angle and the diversity between V_1 and nV_2.

Moreover, the average power that the DAB converter can deliver actually only depends on the products of the fundamental components of the ac voltage and current at the switching frequency and their harmonics with the same orders. The average power then can be calculated.

$$P_{avg} = \sum_{n=1,3,5...}^{\infty} \frac{4V_1 \cdot V_2}{m^3 \pi^2 \omega L_s n} \sin(m\delta). \tag{4}$$

Based on (2)-(4), it is clear that for DAB converters the smaller phase-shift angle and the smaller current slope during δ/ω~π/ω can give less reactive power which circulates in the converter and causes extra loss. Otherwise, more complex modulation schemes such as a phase-shift plus phase-shift method has to be used in order to attenuate the *rms* ac current at a certain average or active power required [10]-[12].

B. Analysis of ac inductor

Based on the typical operating waveforms illustrated in Fig. 3, the flux linkage at the beginning of core saturation is given in (5)

$$\lambda_s = \frac{\Delta\lambda_{\max}}{2} = N_L A_c B_s = \begin{cases} \dfrac{2V_1\delta + \pi(nV_2 - V_1)}{4\pi f_{s\min}} & \text{if } V_1 \leq nV_2 \\ \dfrac{2nV_2\delta + \pi(V_1 - nV_2)}{4\pi f_{s\min}} & \text{if } V_1 > nV_2 \end{cases}. \tag{5}$$

where N_L, A_c and B_s represent the number of turns of the ac inductor, the cross-sectional area of the inductor core and the flux density of the core material, respectively. Accordingly, based upon the pre-defined input and output voltages, output power and switching frequency, the needed minimum cross-sectional area and the number of turns can be calculated and selected to avoid saturating the inductor.

The copper loss or winding loss of ac inductors can be calculated in (6).

$$P_{L,cond} = R_{L,ac} \cdot I_{Lac}^2 \tag{6}$$

where $R_{L,ac}$ represents ac resistance of the winding, and I_{Lac} is the ac *rms* current calculated from (3).

The inductor core losses are estimated using the improved Generalized Steinmetz Equation (iGSE) [13], [14].

$$P_v = \frac{1}{T}\int_0^T k_i \left|\frac{dB}{dt}\right|^{\alpha} (\Delta B)^{\beta-\alpha} dt \,. \tag{7}$$

where P_v is the time-average power loss per unit volume, ΔB is the peak-to-peak flux density, k, α and β are the material parameters, and

$$k_i = \frac{k}{(2\pi)^{\alpha-1}\int_0^{2\pi} |\cos\theta|^{\alpha} 2^{\beta-\alpha} d\theta} \,. \tag{8}$$

From (5)-(8), the dimension of the ac inductor and its associated losses can be calculated and evaluated.

III. Case Study

Nowadays, the DAB converter and the isolated full-bridge bidirectional boost converter (IFB^{3}C) are the two main topologies which can provide galvanic isolation and voltage conversion. In [15]-[17], an IFB^{3}C is investigated to overcome the challenges such as achieving high efficiency over a wide input voltage range for reversible solid oxide electrolyser cells (SOECs). Hereby, in this paper, the same specifications for the IFB^{3}C, as listed in Table I, are used to design the DAB converter and also its ac inductor.

A. Core loss of the ac inductor

Based on the parameters listed in Table I and using (7) and (8), the time-average core loss is:

$$P_v = \frac{2\cdot k_i}{T}\left[\begin{array}{l} \left|\frac{V_1+nV_2}{N_L\cdot A_c}\right|^{\alpha}\left(\frac{V_1+nV_2}{N_L\cdot A_c}\cdot\frac{\delta}{\omega}\right)^{\beta-\alpha}\cdot\frac{\delta}{\omega}+ \\ \left|\frac{V_1-nV_2}{N_L\cdot A_c}\right|^{\alpha}\left(\frac{V_1-nV_2}{N_L\cdot A_c}\cdot(\frac{T}{2}-\frac{\delta}{\omega})\right)^{\beta-\alpha}\left(\frac{T}{2}-\frac{\delta}{\omega}\right) \end{array}\right] \tag{9}$$

Adopting N87 E64/10/50 EI ferrite core in this study, the core loss can be evaluated by both GSE and iGSE methods. When V_1=nV_2=55 V, the core loss as a function of the phase shift angle δ, with varying number of turns, is plotted in Fig. 4. Apparently, the larger number of turns, the higher core loss is.

TABLE I. Specifications for DC-DC Converter Design

Low voltage (LV) side	30-80 VDC
High voltage side	700-800 VDC
Rated power	3 kW
Transformer turn ratio, n	1:14
Ac inductance (LV side)	3 uH
Switching frequency, f_s	100 kHz
Core material	N87 Ferrite
K_c	16.9
α	1.25
β	2.35
B_{peak}	0.49 T

Additionally, the core loss is underestimated by using GSE method, in particular when the phase shift angle is close to $\pi/2$.

Moreover, the core loss is calculated with V_1 of 60 V and V_2 of 700 V by iGSE, which means $V_1 \neq nV_2$ but V_1+nV_2 is kept the same, and hereby the result is plotted in Fig. 5. It can be seen that: due to the second term in the right hand side of (9) the core loss will be even worse; and a large diversity locates in the range with a smaller δ. The core loss as a function of δ and voltage of V_2 can be plotted in Fig. 6. When δ is smaller than $\pi/4$, which is the recommended operating range, the core loss will be minimized under the condition of V_1=nV_2. With lower input voltage, for instance V_1=30V, the core loss can be even smaller than that of V_1=nV_2 when the phase-shift angle is larger. When V_1 is the maximum input voltage of 80V, due to the voltage mismatch compared to nV_2, the core loss increases significantly.

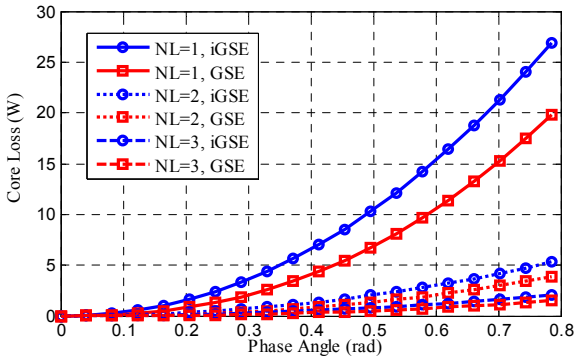

Fig. 4: Core loss as a function of δ with V_1=nV_2.

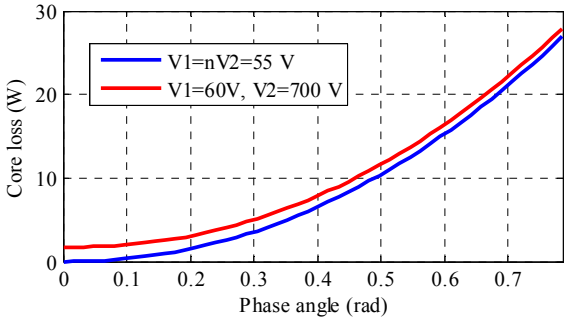

Fig. 5: Core loss with $V_1 \neq nV_2$.

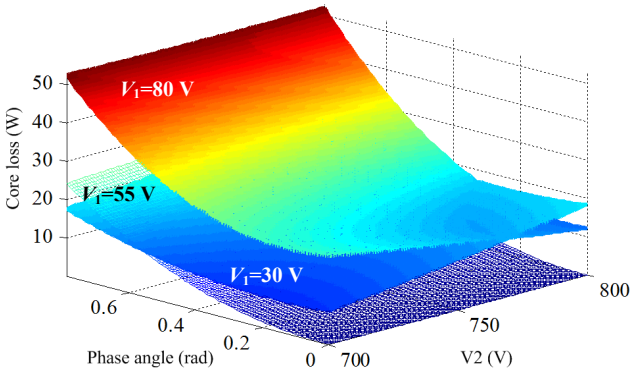

Fig. 6: Core loss as a function of δ and V_2.

B. *Windling loss of the ac inductor*

The ac inductor here has no dc current offset so that is diverse from inductors used as a dc output filter in Buck or Boost converters. Therefore, reduction of ac resistance is the most important issue for obtaining low winding loss. Based on the selected planar core, six winding arrangements defined in Table II respectively, , are compared as illustrated in Fig. 7, in which the yellow bars represent windings, and the ferrite cores are gaped only on the center legs. With Maxwell 2D, these six winding configurations are evaluated and compared in terms of ac resistance. Case 1 to Case 4, and Case 5 and Case 6, can be categorized into two groups, depending on the number of turns.

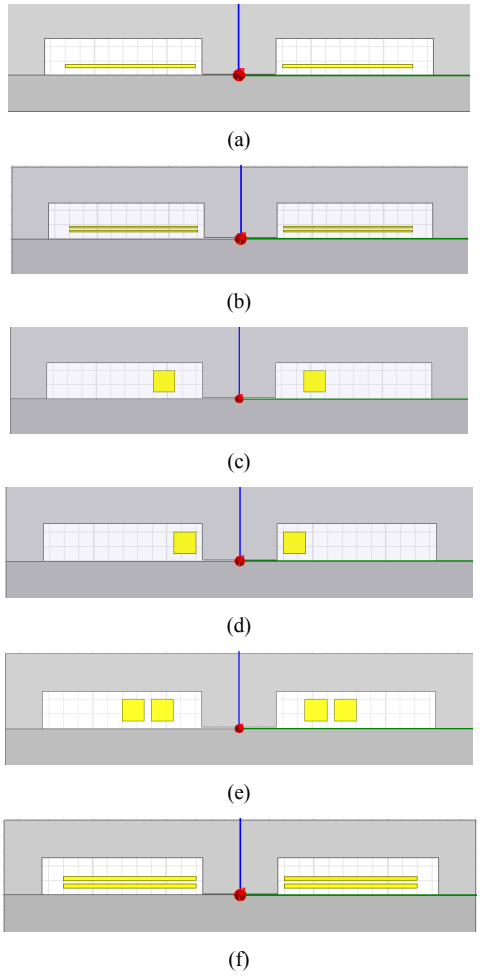

Fig. 7: Winding arrangements. (a) Case 1, (b) Case 2, (c) Case 3, (d) Case 4, (e) Case 5, and (f) Case 6.

TABLE II. WINDING ARRANGEMENT

Case nr.	Winding Configures
Case 1	Single rectangular flat wire
Case 2	Paralleled rectangular flat wires with same cross-section as that in case 1
Case 3	Single square wire with same cross-section as that in case 1 and away from the air-gap
Case 4	Single square wire with same cross-section as that in case 1 and close to the air-gap
Case 5	Two-turn square wire
Case 6	Two-turn rectangular flat wire

In Fig. 8, where only the left parts of the ac inductors are shown due to the symmetrical structure, the FEM analysis results are presented. It can be seen that with a single winding, there are no proximity effect, and accordingly the ac resistance is much smaller than that in the cases of two-turn winding configuration. But the price that must pay for using this single turn inductor with low ac resistance is a relatively large core cross-section area which is needed to avoid core saturation.

Moreover, the fringing flux, due to the air gap in the center leg, can affect the winding loss badly, so the winding must be put at least twice of gap length away from the gap. Finally, the ratios of R_{ac}/R_{dc} are compared in Fig. 9.

C. *Ac inductor design*

With the winding cross-section area of 10 mm^2, the winding losses in the six cases are given in Fig. 10. Comparing to the core loss shown in Fig.5, the cases with a single turn structure can fulfill the optimization criteria, i.e. the core loss is approximately equal to the winding loss, and hereby an ac inductor with only one turn can be designed. If a larger inductance is needed, more ferrite EI cores can be connected in cascade to obtain a larger effective core area, which results in a larger inductance and can avoid saturation effectively.

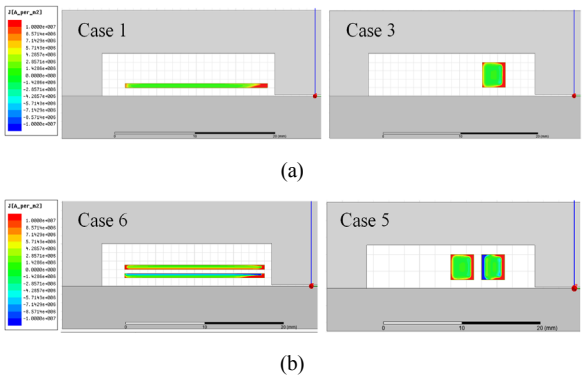

Fig. 8: FEM simulation. (a) Single-turn winding structure, and (b) two-turn winding structure.

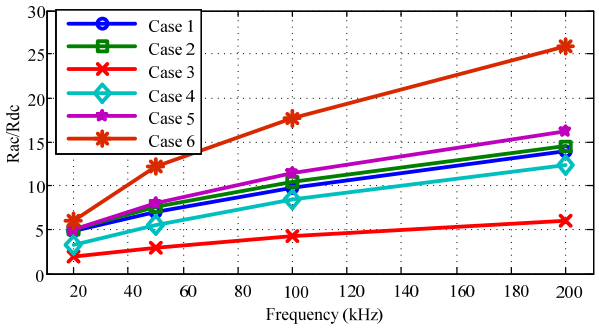

Fig. 9: Comparison of R_{ac}/R_{dc}.

IV. EXPERIMENTAL RESULTS

To verify the proposed ac inductor design, a 3 kW DAB converter has been prototyped. The typical waveforms, i.e. the primary and secondary ac voltages and the ac inductor current of the converter operating at 100 kHz, are given in Fig. 11.

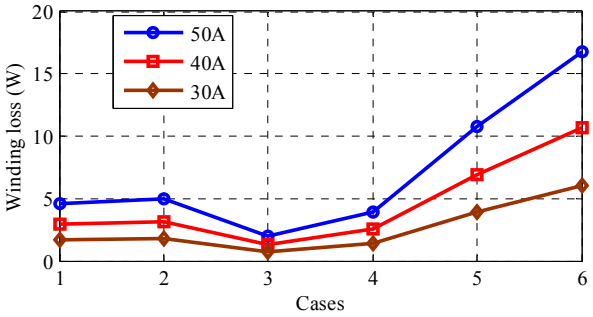

Fig. 10: Winding losses.

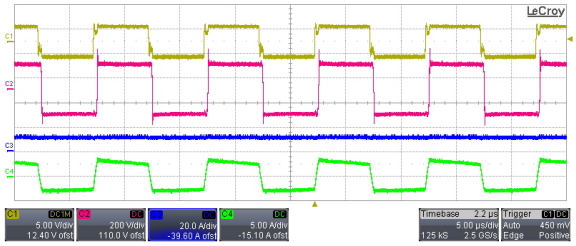

Fig. 11: Experimental waveforms of the DAB converter. CH1: the primary side ac voltage, CH2: the secondary ac voltage, CH3: the input dc current, and CH4: the ac current at the secondary or high voltage side.

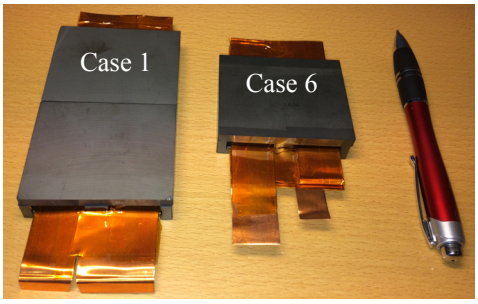

Fig. 12: Ac Inductors of Case 1 and Case 6.

For the purpose of performance comparison, two ac inductors based on the Case1 and Case 6 respectively are built and their photographs are given in Fig. 12, following the parameters listed in Table III. By using Agilent 4294A Precision Impedance Analyzer, the constructed ac inductors are measured in terms of inductance and ac resistance. For the Case 1, the measured inductance and ac resistance at 100 kHz are shown in Fig. 13 (a), in which the values are highlighted with a square in red line. Moreover, the ac resistances of these two inductors at various switching frequencies, i.e. 50 kHz, 100 kHz and 200 kHz are plotted in Fig. 13(b). It can be seen that the Case 1 has smaller ac resistance than Case 6 over the whole frequency band.

TABLE III. AC INDUCTOR DESIGN

	Case 1	**Case 6**
Inductance	3.2 µH	3.2 µH
Core	Planar EI E64/50/10-3C90	
Air gap	0.19 mm	0.46 mm
Number of turns	1	2

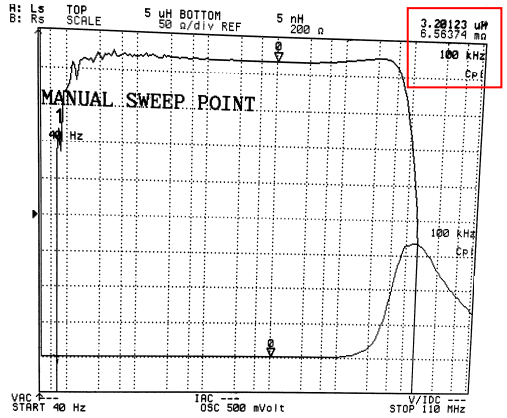

(a)

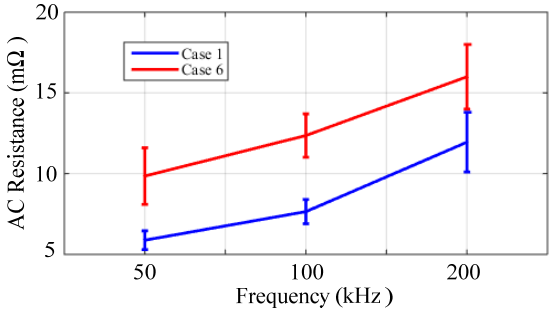

(b)

Fig. 13: Inductance and ac resistance measurement. (a) Measured inductance and ac resistance of Case 1 ac inductor at 100 kHz, and (b) ac resistance comparison of Case 1 and Case 6 at various operating frequencies.

V. CONCLUSION

This paper studied the design of ac inductors employed in the widely used DAB converters. The design difficulty for ac inductors in DAB converters, which operate with a wide input voltage range, has been pointed out and analyzed. Core loss is calculated by the iGSE approach, and the core loss due to input and output voltage mismatch is evaluated. Six diverse winding arrangements and their design are studied and compared with a FEM analysis by Maxwell 2D, and it is found that the ac inductors with a single-turn winding configuration can achieve lowest total losses.

REFERENCES

[1] L. Zhu "A novel soft-commutating isolated boost full-bridge ZVS-PWM DC-DC converter for bidirectional high power applications", *IEEE Trans. Power Electron.*, vol. 21, no. 2, pp.422 -429, 2006

[2] Z. Zhang, O. C. Thomsen, M. A. E. Andersen, "Optimal design of a push-pull-forward half-bridge (PPFHB) bidirectional DC–DC converter with variable input voltage," *IEEE Trans. on Ind. Electron.*, vol.59, no. 7, pp. 2761-2771, Jul. 2012.

[3] S. Jalbrzykowski , A. Bogdan and T. Citko "A dula full-bridge resonant class-E bidirectional dc-dc converter", *IEEE Trans. Ind. Electron.*, vol. 58, no. 9, pp.3879-3883, 2011.

[4] R. Pittini, Z. Zhang, and M. A. E. Andersen, "Isolated full bridge boost dc-dc converter designed for bidirectional operation of fuel

cells/electrolyzer cells in grid-tie applications," *EPE'13-ECCE Europe*, 2013.

[5] Pan Xuewei and Rathore, A.K. "Novel interleaved bidirectional snubberless soft-switching current-fed full-Bridge voltage doubler for fuel-cell vehicles", *IEEE Trans. Power Electron.*, vol. 28, no. 12, pp. 5535 - 5546, Dec. 2013.

[6] Z. Zhang, Z. Ouyang, O. C. Thomsen, M. A. E. Andersen, "Analysis and design of a bidirectional isolated dc–dc converter for fuel cells and supercapacitors hybrid system," *IEEE Trans. Power Electron.*, vol. 27, no. 2, pp. 848 - 859, Feb. 2012.

[7] R. W. De Doncker, D. M. Divan, and M. H. Kheraluwala, "A three-phase soft-switched high-power desity dc/dc converter for high power applications," *IEEE Transactions on Industry Application*, vol. 27, no. 1, pp.63-67, 1991.

[8] S. Inoue and H. Akagi, "A bidirectional dc–dc converter for an energy storage system with galvanic isolation," *IEEE Transactions on Power Electronics*, vol. 22, no. 6, pp. 2299-2306, 2007.

[9] J. Ge, Z. Zhao, L. Yuan and T. Lu, "Energy feed-forward and direct feed-forward control for solid-state transformer," *IEEE Trans. Power Electron.*, vol. 30, no. 8, pp.4042-4047, Aug. 2015.

[10] G. G. Oggier , G. O. Garcia and A. R. Oliva "Modulation strategy to operate the dual active bridge dc-dc converter under soft switching in the whole operating range", *IEEE Trans. Power Electron.*, vol. 26, no. 4, pp.1228-1236, Apr. 2011.

[11] F. Krismer and J. W. Kolar "Efficiency-optimized high current dual active bridge converter for automotive applications", *IEEE Trans. Ind. Electron.*, vol. 59, no. 7, pp.2745 -2760 2012

[12] B. Zhao, Q. Song and W. Liu "Efficiency characterization and optimization of isolated bidirectional dc-dc converter based on dual-phase-shift control for dc distribution application," *IEEE Trans. Power Electron.*, vol. 28, no. 4, pp.1711-1727, Apr. 2013.

[13] J. Muhlethaler, J. Biela, J. W. Kolar and A. Ecklebe, "Improved core-loss calculation for magnetic components employed in power electronics systems," *IEEE Trans. Power Electron.* vol.27, no.2, pp.964-973, Feb. 2012.

[14] W. G. Hurley and W. H. Wolfle, "Transformers and inductors for power electroncis," Wiley, 2013.

[15] R. Pittini, "High efficiency reversible fuel cell power converter," *PhD dissertation*, Techninical University of Denmark, 2015.

[16] R. Pittini, Z. Zhang, and M. A. E. Andersen, "High current planar magnetics for high efficiency bidirectional dc-dc converters for fuel cell applications," in *the 29th Annual IEEE Applied Power Electronics Conference and Exposition (APEC)*, pp. 2641-2648, Fort Worth, TX, USA, 2014.

[17] R. Pittini, M. C. Mira, Z Zhang, A Knott, and M. A. E. Andersen, "Analysis and comparison based on component stress factor of dual active bridge and isolated full bridge boost converters for bidirectional fuel cells systems," in *Power Electronics and Application Conference and Exposition (PEAC)*, pp. 1026-1031, 2014.